Long-term assessment of thermal sustainability of thermoactive geostructures

Yvon Delerablee, Sébastien Burlon, Philippe Reiffsteck

Long term assessment of thermal sustainability of thermoactive geostructures

Y. Delerablee[1], S. Burlon[2], P.Reiffsteck[2]

[1]Antea Group, Antony, 92160, France, yvon.delerablee@anteagroup.com

[2]University of Paris-Est, The French Institute of Science and Technology for Transport, Development, and Networks (IFSTTAR), Marne La Vallée, 77447, France, sebastien.burlon@ifsttar.fr, philippe.reiffsteck@ifsttar.fr

Abstract

Thermoactive geostructures represent an original and efficient technique to fulfil energy demand of buildings and infrastructure, both in terms of cooling and heating. Thermal and mechanical aspects have to be considered to achieve a proper design of such structures. This paper only focuses on thermal aspects and deals with the development of an original approach based on the analysis of thermal flux and volumetric thermal power to assess the thermal sustainability of a thermoactive geostructure. This approach is firstly applied to a simple 3D geometry to validate some numerical implementation issues. A case study based on a Grand Paris Express metro station is then presented and analysed in terms of temperature variations and heat exchanges. For each case, several thermal solicitations are considered and the ground response is calculated. The consideration of the groundwater flow and the thermal exchanges by conduction and advection provides a new and better insight of the thermoactive geostructure energy assessment. Indeed, this approach permits the estimation of the contribution of heat exchanges by conduction and advection and the decrease of the design uncertainties related to the ground thermal conduction properties and the groundwater flow velocity. Furthermore, the obtained numerical results show the zones of the geostructures where the heat exchanges are the most significant and where the risk of temperature drift is the highest. This analysis can be used to improve the design of the thermoactive metro station.

Keywords: Diaphragm & in situ walls, Energy, Environmental engineering, Finite-element modelling

Introduction

Thermoactive geostructures have been still in great development since their creation during the years 1980s, especially in European countries (Brandl, 2006) where the use of renewable energy in urban areas is of major importance. Even though the implementation of thermoactive geostructures is gaining more acceptance, there are still some issues related to the thermo-hydro-mechanical behaviour of the ground and the thermo-mechanical behaviour of the structure, which restricts the development of efficient and unambiguous design procedures. For example, in France, the Société du Grand Paris, in charge of the Grand Paris Express project including more than 200 km of tunnels and 68 new metro stations, facilitates the use of thermoactive diaphragm walls for some metro stations but demands a reliable design proving the sustainability of such structures at least for 30 years. Two specific issues have to be properly addressed: the long term thermal performance and the effect on the ground temperature. Many studies have been carried out to improve the understanding of the thermo-mechanical behaviour of the ground (Campanella and Mitchell, 1968; Laloui and Cekerevac, 2008) and the thermoactive geostructures, especially energy piles (Bourne-Webb et al, 2009; Adam and Markiewicz, 2009; Di Donna et al, 2016). Many design elements are also existing but there is still a lack of precise design procedures.

Regarding the thermal design, a lot of information is available for borehole heat exchangers and energy piles and many solutions have been developed based on the infinite line source theory (Ingersoll et al., 1954). Now, g-functions are used to take into account the effects of the radius and the length of these heat exchanger elements: the heat source is finite and its radius is not equal to zero. Superposition approaches are performed to account for spatial and transient aspects (Man et al., 2010, Loveridge and Powrie, 2013). Moreover, some approaches have been developed for the modelling of thermal response tests (Signorelli et al, 2007; Zarrella et al, 2017) and can obviously be applied to thermoactive geostructures (Xia et al, 2012). As highlighted by Bourne-Webb et al. (2016), there are few analytical solutions available for energy diaphragm walls and in most cases numerical methods are used.

Regarding these numerical methods, an important issue concerns the scales where heat exchanges occur. At least, two different scales can be distinguished: a local scale to characterise the heat pump

performances and the heat transfers between the heat-transfer fluid and the pipes located into the thermoactive geostructure (Pahud et al, 1999). Many phenomena have to be considered such as the type of flow which can be laminar or turbulent. The characteristic time and space scales are very small. A larger scale can be defined and concerned the overall thermoactive geostructure where heat exchanges are governed by (i) the thermal conduction through the concrete and the surrounding ground, (ii) the groundwater flow velocity that affects the thermal recovering and the thermal exchanges by advection (Fromentin et al, 1997, Barla et al, 2016), (iii) the influence of the external air temperature and (iv) the three dimensional shape of the geostructure itself that can affect the groundwater flow inducing some dam effects. These two simulation scales require to be addressed separately in order to avoid too long computation times.

In terms of design, four major issues should be addressed: the long-term effects on the ground temperature, the assessment of the thermal power exchanged between the ground and the thermoactive geostructure, the contributions of the conduction and the advection according to the groundwater flow velocity and the influence of each wall in the heat exchanges. The long-term behaviour of such structure is closely link to the mean thermal drift year after year. Indeed, if the temperature of the ground globally decreases or increases year after year, the temperature of the heat carrier fluid will follow this trend to ensure thermal exchange and the thermal performance of the system will decrease (Pahud et al, 1999).

In this paper, an original approach is developed to assess the thermal sustainability of thermoactive geostructures at a large scale. This approach is based on the study of the conductive and advective thermal fluxes. The energy balance equation is presented and analysed to introduce this new approach. Heat exchanger tubes embedded into the diaphragm walls are simulated using finite lines source. In each line, a part of the total energy demand is applied. A first simple example is presented to illustrate the main advantages of this approach and its capacity to assess the conductive flux and the advective flux respectively. This analysis can provide some elements to decrease the design uncertainties related to the ground thermal conduction properties and the groundwater flow velocity.

The second example is based on a Grand Paris Express metro station. For each case, the ground response is calculated according to the thermal solicitation of the structure.

1. Proposed thermal design procedure for metro stations

1.1. Heat exchange assessment

In the case of thermoactive diaphragm walls, the study of thermal exchanges requires to consider 3D effects, especially those related to the groundwater flow. Indeed, geotechnical structures as diaphragm walls modify water levels and flow velocities, inducing dam effects. These modifications of the groundwater flow affect the heat fluxes that are not the same in all the directions around the structure.

In a numerical model, some local variables can be calculated: the heat flux $\vec{j}(x,t)$ (W/m²), the divergence of the heat flux $div(\vec{j}(x,t))$ (W/m^3), the temperature $T(x,t)$ (K), the groundwater flow velocity $\vec{v}_D(x,t)$ (m/s), etc. Moreover, some global variables at the structure scale can be calculated: the heat global exchange $P_{tot}(\mathrm{t})$ (W) and the mean global heat flux $\Phi(t)$ (W/m²) (see Figure 1 for the example of a metro station), the thermal drift, etc. It is also possible to define temporal mean values, as the daily annual mean of global heat exchange $\bar{P}_{tot,year}$ ($W_{day/year}$) and the seasonal annual mean of heat fluxes $\bar{\Phi}_{year}$ ($W/m^2{}_{3month/year}$).

In order to evaluate properly the thermal exchanges between the ground and the thermoactive geostructure, the energy balance equation (see Appendix 1) can be used to identify the terms accounting for the conduction and the advection at a local scale. By means of the differential operator "divergence", it is possible to calculate at a global scale the heat global exchange $P_{tot}(\mathrm{t})$ (W). Thanks to the Green-Ostrogradski's theorem, also called divergence theorem or Gauss's theorem, it is possible to link the divergence of the flux and the flux themselves (see Equation 1).

$$\oiint_{\partial v} \vec{j} \cdot dS = \iiint_{v} \vec{\nabla} \cdot \vec{j} dV \quad (1)$$

The calculation of the divergence allows the calculation of the inlet and outlet fluxes from a ground volume. This is also a way to study temperature variation: when the sign of the divergence is negative

(resp. positive), the temperature is increasing (resp. decreasing). The higher the divergence is, the faster the increase is. Moreover, if steady state is reached, the following equation is obtained:

$$div(\vec{j}_{cond}) + div(\vec{j}_{adv}) = 0 \quad (2)$$

When the sum of the divergence is zero, there is no temperature variation in the system.

The link between the divergence flux and the heat flux can be efficiently used to define a ground volume embracing the whole structure in order to assess the heat transfers in every direction. As the ground volume impacted by the thermoactive geostructure is unknown at this stage, many control volumes can be defined (Figure 2). In a first approach and for the case of thermoactive diaphragm, the impacted volume of ground should be low due to the dam effect and the dimensions of the structure. Thereby, three control volumes are defined:

- Control volume 1 which correspond to the walls;
- Control volume 2 which correspond to the interface ground/structure (i.e. 0-1 m);
- Control volume 3 which correspond to the ground far from the structure (i.e. 1-5 m).

The heat diffusion through each control volume by the mean of the operator 'divergence' can be analysed. Each control volume includes many sub-zones (Figure 2) generated during the discretization of the mesh. Integration of all sub-zones of the Divergence Contact Volume DCV corresponds to the whole heat transfer from the geostructure to the ground P_{tot}.

$$div\left(\vec{j}_{tot,i}(t)\right) = div\left(\vec{j}_{cond,i}(t)\right) + div(\vec{j}_{adv,i}(\mathrm{t})) \text{ at any point} \quad (3)$$

$$P_{tot}(\mathrm{t}) = \sum_{i=1}^{n} V_i div\left(\vec{j}_{tot,i}(t)\right) \text{ for the control volume} \quad (4)$$

where $P_{tot}(\mathrm{t})$ is the global heat exchange through the DCV (W), n is the number of sub-zones of the DCV and V_i the volume of sub-zone i (m^3). If the results show a thermal diffusion more widespread, more DCV can be defined.

To deal with 3D issues, the DCV approach is applied on two examples with an increasing level of complexity. In each example, the effects of various assumptions issues are studied: the geometry, the boundary conditions, the geology, the ground properties and the energy demand with various kinds of

thermal solicitations. A map of divergence values is also presented. This map highlights the zones where the risk of thermal drift is the highest.

1.2. Thermal solicitations assumptions

It is essential to note that the input data in terms of thermal solicitations is the energy demand of the building for heating and cooling taking into account the contribution of the Ground Source Heat Pump GSHP. This thermal signal is applied as a power in each node of the finite line sources located in a same plane for each diaphragm wall (see Figure 3).

Since the energy demand of a building is uncertain during the design process, two shapes of thermal solicitations are tested: a sinusoid and a real one based on a hourly demand. Moreover, hydraulic properties suffer from a considerable uncertainty and imply to consider at least two types of groundwater flows. All the numerical calculations are performed with the finite-difference software FLAC3D (ITASCA, 2012).

2. Example 1: simple 3D case

2.1. Geometry, ground conditions and boundary conditions

The structure includes four thermoactive diaphragm walls with the same dimensions and a non-activated base slab. The diaphragm walls are extended above the top of the model to simulate the boundary conditions on the upper part of the walls. At their base, the diaphragm walls are installed in an impermeable layer to reduce vertical hydraulic flux. The groundwater flow is perpendicular to one side of the metro station.

The ground is composed by two layers. Both layers are homogenous with isotropic properties. The upper layer corresponds to a mean permeable soil and the lower layer represents the impermeable substratum. The ground is fully saturated below the water table and dry above it. The groundwater flow is governing by the Darcy law (see Equation 5).

$$\vec{v}_D = -k \times i \tag{5}$$

where $\vec{v}_D$ is the groundwater flow velocity (m/s), k the hydraulic conductivity (m/s) and i the hydraulic gradient (m). Moreover, the hydraulic gradient is defined as:

$$i = \frac{\Delta h}{D} \quad (6)$$

where Δh is the difference of water head between the two boundaries downstream and upstream (m) and D the total length between these two boundaries (m). Furthermore, the variation of groundwater temperature can create heat-driven flow due to the variation of density (Philip and De Vries, 1957; Crausse, 1983). However, the thermal gradient and the range of temperature are relatively low for thermoactive diaphragm wall. It means that, in this case, there is no heat-driven flow (Daghari and De Backer, 2000).

The mesh is composed of hexahedrons, including 178 233 nodes and 171 200 zones and is refined close to the ground-structure interface to assess more precisely the heat transfers between the ground and the concrete. The time step is 720 seconds, which permits to account for transient effects.

At the bottom boundary, the temperature is fixed to the mean annual temperature T_{ave} and the hydraulic flux is null. On the edges boundaries, the temperature and the water head are constant. At the surface boundary, the temperature is imposed according to a sinusoidal signal described by Equation (7):

$$T(z,t) = T_{ave} + A_T \times \left(sin(\omega \times t)\right) \quad (7)$$

where T_{ave} is the annual average temperature (°C), A_T the maximum annual amplitude of temperature (°C), ω the annual radial frequency (s^{-1}) and t the time (s).

The thermal fluxes induced by the temperature variation at the surface is an important parameter to consider. Indeed, the ground may be divided into three thermal zones (Burger et al, 1985):

- the heterothermal zone (0-15 m): the temperature varies with time and depth;
- the neutral zone (15-50 m): the temperature is equal to the annual average temperature;
- the homothermal zone (below 50 m): the effect of geothermal gradient becomes prominent.

Thermoactive geostructures are most of the time only concerned by the heterothermal and the neutral zones because of their low depth (≤ 50 m). The temperature distribution in these zones can be described by Equation (8).

$$T(z,t) = T_{ave} + A_T \times e^{-(z/d)} \left(sin\left(\omega \times t - \frac{z}{d} \right) \right) \quad (8)$$

where z is the depth (m) and d the damping depth of annual fluctuation (m).

In metropolitan France from 1981 to 2010, the annual mean temperature of the atmosphere is between 12°C to 14°C (METEO FRANCE, 2018). Thus, in France, the ground temperature range in the neutral zone is between 12°C to 14°C. These values are true for undisturbed area but do not take into account heat island or other local phenomena (Menberg *et al*, 2012). Figure 4 represents an example of the seasonal analytical temperature profiles. As the heat flux is proportional to the temperature gradient, the heterothermal zone can modify the heat exchanges between the energy diaphragm walls and the ground. Thereby, the ground temperature over the depth is non-homogenous and the heat fluxes are not only horizontal all over the system (Spitler and Gehlin, 2015).

Furthermore, a convective heat flux boundary condition is imposed to consider heat transfers between the internal air of the metro station and the concrete of the diaphragm walls and the base slab. As there is no hydraulic flux through the diaphragm walls, the heat transfers in the concrete is only conductive. Concerning the heat transfers into the ground, it follows the conductive and advective laws described in Appendix 1.

Figure 5 and Table 1 show the geometry and the boundary conditions. To limit the size of the model and to observe a local thermal plume, the hydraulic conductivity is medium. All the material properties are listed in Table2.

2.2. Initial conditions

It is of major importance to initialise the whole model in terms of temperature and groundwater flow velocity. The first step concerns the groundwater flow and highlights the dam effect imposed by the

structure (see Figure 6), which is low in this case. Indeed, the water head slightly increases upstream and slightly decreases downstream of the structure. In the area close to the metro station, variations of the free surface level reach 10 cm. However, Figure 7 shows the decrease of the groundwater flow velocity close to the metro station faces perpendicular to the hydraulic flux (walls 1 and 2) where it reaches a value close to zero. At the corners of the station, there is an increase of the groundwater flow: the velocity value is between 1.5 to 2 times larger than the undisturbed velocity value. As the heat flux by advection depends on the hydraulic flux (see Equation A1.6.a), the zones where the hydraulic flux is null are purely conductive and the zones where the hydraulic flux is the highest dissipate more heat. The second step aims at the initialisation of the ground temperature according to the seasonal temperature variation at the ground surface and the convective heat transfer between the internal air of the station and the diaphragm walls.

After these two steps, regarding to the hydraulic flux field, some faces are much more dissipative than the others and, as shown by Figure 8, a thermal plume occurs in the first twenty meters downstream. The thermal field around each face of the structure is different and, as expected, the heat flux between each face and the soil is different.

2.3. Thermal solicitation

An important issue for the thermal design is the choice of the energy demand since it depends on many parameters as the building type (office, house, etc.), the policy regulation, the construction materials, the insulation, etc. It is important to ensure that the global energy demand is balanced on one year or that the natural thermal recharge is sufficient to avoid thermal drift. A balanced demand is usually met for office building but rarely for house where heating is dominant. According to the type of building, a ratio of power by living area can be predicted. Another solution is to consider typical heat flux met with thermoactive geostructures from literature (Fromentin et al, 1997; Brandl, 2006), for example, 30 W/m² for thermoactive diaphragm walls.

Different shapes of signals for energy demand have been tested: a sinusoid and a real design energy demand based on hourly values. The sinusoid is perfectly balanced and the increase of energy demand is smooth. The other one considers thermal rest and large peaks of demand which can be defined according to the type of the building, its insulation, etc.

In this example, a sinusoidal thermal solicitation signal is tested considering an hourly demand in kWh/h (Figure 9). The signal starts from zero, representing the season of thermal recovery of the ground, i.e. when the building does not need neither heating nor cooling. In this case, it starts in spring with an injection of heat into the ground for cooling. Each finite line source is composed by 26 nodes and spaced of 1.5 m from the others. The value imposed at each node depends on the total power and the total number of nodes of the finite lines sources defined previously:

$$Q_{node} = \frac{Q}{n_{node}} \quad (9)$$

where Q_{node} is the value of energy demand imposed on one node (kWh/h), Q is the total value of energy demand (kWh/h) and n_{node} is the number of nodes where the energy demand is imposed.

2.4. Results

Figure 10 presents a cross section of the divergence map at the end of July during the year 5 at 9 m depth: the temperature of the ground is increasing when divergence values < 0 (W/m^3) and decreasing for divergence values > 0 W/m^3. It is interesting to note that the temperature of the ground close to the wall 1 is decreasing while the thermal solicitation induces an increase of temperature into this wall. In fact, the groundwater flow tends to limit the temperature variations in the ground. This figure also shows two seasonal thermal waves downstream.

Figure 11 shows the results of 5 years of activation in terms of heat exchanges for each wall. It is important to notice that the heat exchange calculated with this method is a balance of energy between an inside and an outside flux. The results show that globally on one year, the temperature of the ground decreases close to the walls and the walls 1 is the most dissipative. This temperature variation

tends to decrease along the time and the heat exchanges move towards an equilibrium. Finally, there is no thermal drift around the structure.

Figure 12 shows the heat fluxes at the interface ground/structure at the end of July of the first year. Each point corresponds to one position on the wall. These values are quite sensible according to the experience. The zones above the base slab are much more productive than the zones below that include the zones between the four diaphragm walls and the zones outside the structure. It can be explained by the seasonal variation of the external air temperature (see section 2.1). It also shows that the wall 1 is the most productive. The walls 3 and 4 are very similar in terms of heat exchange due to the symmetry of the model. Globally, the wall 2 is less productive than the others.

Figure 13 illustrates the heat diffusion through the three DCV (see Figure 2) of the model during the third year of activation. In terms of global heat exchange P_{tot}, it shows the diffusion shift between each volume: the DCV 1 is the first to react to the thermal solicitation but after few days, the DCV 2 is the most dissipative volume. It can be explained by the fact that the heat exchanger tubes are close to the ground/structure interface (20 cm), so the concrete is quickly saturated by the thermal solicitation. Thereby, the DCV 2 is the biggest reservoir of heat in this example, followed by the DCV 1 and the DCV 3. In this last volume, the temperature varies with a delay of 1 to 2 months regarding to the thermal solicitation and the mean global heat fluxes is low. When the peak of demand is the highest (t = 2190 h and t = 6570 h), the sum of the heat global exchanges in the DCVs 1, 2 and 3 is equal to the thermal solicitation. Regarding the mean global heat fluxes, as the zone below the base slab between the diaphragm walls are considered, low values are taken into account explaining the low global values in average.

3. Example 2: typical Grand Paris Express metro station

3.1. Geometry, ground conditions and boundary conditions

Paris geology is very well known due to its great urbanisation (Figure 14). The ground is composed by many sedimentary layers as sand, marl, clay and limestone. Regarding the hydrogeology, three

aquifers, in six ground layers, mainly concern thermoactive geostructures: the Saint Ouen Calcareous rocks and the Beauchamps Sands, the Marls and Rocks and the Coarse Calcareous Stones, the Cuise Sands and the Chalk.

For this case study, the thermal and hydraulic properties are listed in Table 3. These values are chosen as average values. These layers are favourable to thermal exchanges regarding their thermal and hydraulic conductivity. They are homogenous with isotropic properties. The most permeable layer is the "Marls and Rocks", which mean that this layer is the most productive in terms of heat exchanges thanks to the advective heat flux.

The boundary conditions are similar to those used in example 1 (see section 2.1). On the bottom boundary, the temperature is fixed to the mean annual temperature T_{ave} and the hydraulic flux is null. The edges boundaries are at constant temperature and the water head is imposed respectively to the hydraulic gradient in order to initialise a groundwater flow perpendicular to the longest side of the structure. On the surface boundary, the temperature is imposed respectively to the seasonal temperature variation of the external air. Furthermore, a convective heat flux boundary condition is imposed to consider heat transfer between the internal air of the structure and the concrete.

The geometry and the boundary conditions of the metro station model are described in Figure 15 and Table 4. The Coarse Calcareous Stones represents the substratum. In this case, the diaphragm walls are quite deep and large, which let suppose that their impact on groundwater flow is not negligible.

In comparison to the example 1, the hydraulic conductivity is high in specific ground layers, which implies that the boundaries must be set up far away downstream to let the thermal plume expand. Alternatives periods in terms of heating and cooling demand create seasonal thermal waves. The goal is to absorb these thermal waves after some cycles, i.e. 4-5 years, to limit the model dimensions.

As there is no hydraulic flux through the diaphragm walls, the heat transfers in the concrete is only conductive. Concerning the heat transfers in the ground, it follows the conductive and advective laws described in Appendix 1. To deal with uncertainties on hydraulic conditions, two different hydraulic

gradients are tested: 0 % and 0.38 %. The water head downstream and upstream are imposed to create these two hydraulic gradients. Thus, for the second case, the water head difference is 2 m for a total length of 530 m. The mesh in composed by hexahedrons and is refined close to the diaphragm walls and it includes 411450 nodes and 398800 zones. The time step is 720 seconds to account for transient effects.

3.2. Initial conditions

The initialisation of the model follows the same procedure as in example 1. Since the geology is composed by different layers, the groundwater flow is variable and depends on the hydraulic conductivity of each layer. Moreover, the first meters of the model are dry. Figure 16 shows the dam effect caused by the structure for the two different hydraulic gradients considered. The case of null hydraulic gradient does not suffer from dam effect and in the case of hydraulic gradient equal to 0.38 % it is low and the variations of the free surface level reach 10 to 15 cm. As in example 1, the corners of the diaphragm walls are the zones where the groundwater flow velocity is the highest and the groundwater flow velocity close to the upstream and downstream walls is close to zero. Figure 17 shows the temperature field around the structure. The symmetry of the thermal field can be explained by the low hydraulic conductivity of the upper ground layers which prevent the formation of a thermal plume.

3.3. Thermal solicitations

In this example, the sinusoidal and the real signals based on design demands are used (Figure 18). The signal starts from zero, representing the season of thermal recovery of the ground, i.e. when the building does not need neither heating nor cooling. In this case, it starts in spring with an injection of heat into the ground for cooling. The real energy demand is unbalanced with more heating than cooling and the demand is null during the weekends and low during the nights. Each finite line source is composed by 54 nodes and spaced of 2 m from the others.

3.4. Results

The results analysed in this section come from a 10-years calculation.

In the case of the sinusoidal signal, regarding the heat exchange based on the divergence approach (see Figure 19) the temperature globally decreases into the ground close to the diaphragm walls and the walls 1 and 2 are the most dissipative. After five years, the system reached a steady state. Figure 20 shows different cross section of the heat flux divergence at different depths (20 m and 40 m). It appears that the divergence is variable according to the kind of layer. Around the structure in the layer where the hydraulic flux is low (case a), the divergence is mainly conductive and the dissymmetry is low. Nevertheless, in the layer with high hydraulic conductivity (case b) and in the corner of the diaphragm walls, the divergence of the advective heat flux is non-negligible and correspond to 30 % of the total heat exchange. Thereby, the part of heat exchange close to the structure is essentially conductive but locally, the advection has a non-negligible impact. These cross-sections also highlight the zones where the heat is stored year after year. It appears that the groundwater flow is not necessarily a favourable parameter. Indeed, in the case of a sinusoidal thermal solicitation, the energy demand is balanced and heat is stored in the ground in summer and extracted during winter. However, the groundwater flow dissipates the heat stored in the ground seasons after seasons. In this example, the upstream and downstream walls contribute to store heat and the edge walls to dissipate heat. Thereby, the minimum and maximum temperatures are reached in the ground close to the edge of the structure (see Figure 21).

In the case of the real energy demand, the study of the heat flux divergence (see Figure 22) clearly depicts the unbalanced energy demand. Indeed, $\bar{P}_{tot}$ is positive and is increasing, inducing a decrease of the temperature around the structure. The decrease rate of the ground temperature is lower and lower with time and does not reach an asymptote after 10 years. The wall 1 is the most dissipative. The walls 3 and 4 less suffer from thermal drift, probably due to the groundwater flow which dissipates the thermal anomaly. This behaviour is also noticeable on the heat fluxes between the diaphragm walls and the ground. Indeed, the decrease of temperature reduces the heat flux with time (Figure 23 for

wall 1 and Figure 24 for wall 4). For the wall 1, the decrease of the heat fluxes reaches approximately 10 % in autumn against 5 % for the wall 4 after 10 years. The decrease is dependant of the season due to the shape of the signal.

Conclusions

Thermoactive diaphragm wall design suffers from the lack of studies related to the effects of groundwater flow and the heat diffusion into the ground. The original approach presented in this paper is based on the study of the heat flux divergence giving some insights about the behaviour of such structures. At a local scale, the 'divergence' operator is a reliable parameter to analyse the temperature variations into ground volumes and the thermal waves caused by the seasonal energy demand. Moreover, conduction or advection contributions in terms of heat exchanges can be clearly identified. At a larger scale, the 'divergence' operator shows the temperature evolution into the various control volumes (DCVs). For a metro station, the contribution of each wall can be assessed, which permits to choose the walls where the heat exchanger tubes have to be installed in order to optimise the heat exchanges. In presence of groundwater flow, the calculation shows that the thermal contribution of each wall is different due to the advection effects. Temperature variations imposed by the heat exchanger tubes are dissipated, which induces a thermal plume. When the thermal solicitation is unbalanced, the groundwater flow decreases the thermal drift close to the structure and allows more heat exchanges. As a conclusion, for thermoactive diaphragm walls, the calculations performed show that the heat exchanges are mainly conductive due to the dam effect but the groundwater flow induces a favourable thermal gradient for the upstream wall.

Acknowledgments

This work was carried out in the framework of the COST Action GABI TU 1405, European network for shallow geothermal energy applications in buildings and infrastructures. The authors thank all the participants to this European project for the interesting and fruitful discussions.

Nomenclature

A	Constant [m^{-1}]
A_T	Maximum annual amplitude of temperature [K]
C	Specific Heat [J/kg.K]
C_v	Volumetric specific heat [$J/m^3.K$}
d	Damping depth of annual fluctuation [m]
D	Total length [m]
div(j)	Divergence of heat flux [W/m^3]
DCV	Divergence Contact Volume
GSHP	Ground Source Heat Pump
h	Water head [m]
i	Hydraulic gradient
j	Heat flux [W/m^2]
k	Hydraulic conductivity [m/s]
L	Characteristic length [m]
n	Porosity [-]
P	Power balance [W]
P_e	Peclet number [-]
Q	Energy Demand [kWh/h]
S	Surface [m^2]
Sr	Saturation [-]
T	Temperature [°C]
t	Time [s]
v_D	Groundwater flow velocity [m/s]
V	Volume [m^3]
z	Depth [m]

Greek symbols

∇T	Thermal gradient [K/m]
λ	Thermal conductivity [W/m.K]
ρ	Density [kg/m^3]
ω	Annual radial frequency [s^{-1}]

Subscripts

adv	Advection
ave	Annual average
cond	Conduction
d	dry
eff	Effective
int	internal
n	Number of zone
sol	solid
tot	total
w	water

Bibliography

Brandl H. (2006). Energy foundations and other thermo-active ground structures. *Géotechnique*, **56**(2): 81-122.

Campanella R.G. & Mitchell J.K. (1968) Influence of temperature variations on soil behavior. *Journal of soil mechanics and foundation division ASCE*, **94**(3): 709-734.

Laloui L., & Cekerevac C. (2008). Numerical simulation of the non-isothermal mechanical behavior of soils. *Computers and Geotechnics*, **35**: 729-745.

Bourne-Webb P.J., Amatya B., Soga K. (2009). Energy pile test at Lambeth College, London: geotechnical and thermodynamic aspects of pile response to heat cycles. *Géotechnique*, **59**(3): 237-248.

Adam D., & Markiewicz R. (2009). Energy from earth-coupled structures, foundations, tunnels and sewers. *Géotechnique*, **59**(3): 229-236.

Di Donna A., Rotta A.F., & Laloui L. (2016). Numerical study of the response of a group of energy piles under different combinations of thermo-mechanical loads. *Computers and Geotechnics*, **72**: 126-142.

Ingersoll L.R., Zobel O.J., Ingersoll A.C. (1954). Heat conduction with engineering and geological applications. 3rd Edition. New York: McGraw-Hill.

Man Y., Yang H., Diao N., Liu J., Fang Z. (2010). A new model and analytical solutions for borehole and pile ground heat exchangers. *Intl. J. Heat Mass Transfer,* **53**(13–14):253–2601.

Loveridge F. and Powrie W. (2013). Temperature response functions (G-functions) for single pile heat exchangers. Energy; **57**(August):554–64.

Signorelli S., Bassetti S., Pahud D. & Kohl T. (2007). Numerical evaluation of thermal response tests. *Geothermics*, **36**: 141-166.

Zarella A., Emmi G., Zecchin R. & De Carli M. (2017). An appropriate use of thermal response test for the design of energy foundation piles with U-tube circuits. *Energy and buildings*, **134**: 259-270.

Xia C., Sun M., Zhang G., *et al*. (2012). Experimental study on geothermal heat exchangers buried in diaphragm walls. *Energy and Buildings*, **52**: 50-55.

Bourne Webb P., Burlon S., Javid S., Kuerten S. and Loveridge F. (2016). Analysis and design methods for energy geostructures. *Renewable & Sustainable Energy*, **65**, 402-419.

Pahud D., Fromentin A., & Hubbuch M. (1999). Heat exchanger pile system of the dock midfield at the Zürich Airport. Detailed simulation and optimization of the installation. *Rapport final. Rapport d'étude n°120.110*. Office fédéral de l'énergie, Lausanne, Suisse. 49 p.

Fromentin A., & Pahud D. (1997). Recommandations pour la réalisation d'installations avec pieux échangeurs. Rapport final. *Rapport d'étude n°120.104*. Office fédéral de l'énergie, Lausanne, Suisse. 79 p.

Barla M., Di Donna A. & Perino A. (2016). Application of energy tunnels to an urban environment. *Geothermics*, **61**: 104-113.

ITASCA. (2013). FLAC3D Version 5.01 User's guide. Minnesota, USA: ITASCA Consulting Group, Inc.

Philip J.R., & De Vries D.A. (1957). Moisture movement in porous materials under temperature gradients. *Transactions – American Geophysical Union*, **38**(2): 222-232.

Crausse P. (1983). Etude fondamentale des transferts couplés de chaleur et d'humidité en milieux poreux non saturés. Thèse de doctorat, Institut National Polytechnique, Toulouse, 209 p.

Daghari H., & De Backer L. (2000). Water movement in non isothermal porous medium. *Revue des sciences de l'eau*, **13**(1): 75-84.

Burger A., Recordon E., Bovet D., Cotton L. & Saugy B. (1985). Thermique des nappes souterraines. Lausanne: Presses Polytechniques Romandes.

METEO France. (2018). http://www.meteofrance.fr/climat-passe-et-futur/bilans-climatiques (consulted the 17/09/2018).

Menberg K., Bayer P., Zosseder K., Rumohr S. and Blum P. (2012) Subsurface urban heat islands in German cities. Science of the Total Environment 442, 123-133

Spitler J.D., & Gehlin S.E.A. (2015). Thermal reponse testing for ground source heat pump systems –An historical review. *Renewable and Sustainable Energy Reviews*, **50**: 1125-1137.

Crank J. (1975) The Mathematics of Diffusion, 2nd Ed. Oxford: Oxford University Press.

Appendix 1: Energy balance equation analysis

The power balance equation used to assess the thermal exchanges between the ground and the thermoactive geostructure including conduction and advection effects is the following (Crank, 1975):

$$C_{eff}\frac{\partial T}{\partial t} + div(\vec{j}_{cond}) + div(\vec{j}_{adv}) - j_{int} = 0 \quad \text{(A1.1)}$$

where C_{eff} is the effective specific heat (J/m^3.K), T the temperature (K), $\vec{j}_{cond}$ the conductive heat flux (W/m^2), $\vec{j}_{adv}$ the advective heat flux (W/m^2) and j_{int} the internal volumetric heat source intensity (W/m^3). The effective specific heat is defined as:

$$C_{eff} = \rho_d C_v + nS_r\rho_w C_w \quad \text{(A1.2)}$$

where ρ_d and ρ_w are respectively the solid matrix bulk density and the density of water (kg/m^3), C_v and C_w are respectively the bulk specific heat and the specific heat of water (J/kg.K), n the porosity (-) and S_r the saturation (-).

The first term $C_{eff}\frac{\partial T}{\partial t}$ corresponds to the thermal inertia of the system, i.e., the quantity of energy needed to vary the temperature over time. The second term $div(\vec{j}_{cond})$ represents the part of conduction during heat transfer while the third term $div(\vec{j}_{adv})$ is the part of advection in heat transfer. The last term concerns the production of internal heat by materials. This term is related to the geology and the depth considered according to the geothermal gradient. In this study, the geology is composed by materials with low heat production as sand and calcareous rocks and a normal geothermal gradient. Therefore, this term is neglected in this study. Regarding to these elements, Equation (A1.1) becomes:

$$C_{eff}\frac{\partial T}{\partial t} + div(\vec{j}_{cond}) + div(\vec{j}_{adv}) = 0 \quad \text{(A1.3)}$$

According to the Fourier's law:

$$\vec{j}_{cond} = -\lambda_{eff} \cdot \nabla T \quad \text{(A1.4)}$$

where λ_{eff} is the effective thermal conductivity (W/m.K). The effective thermal conductivity is defined as:

$$\lambda_{eff} = \lambda_{sol} + nS_r\lambda_w \quad \text{(A1.5)}$$

where λ_{sol} and λ_w are respectively the solid thermal conductivity and the water thermal conductivity.

Considering that the water is incompressible ($div(\overrightarrow{v_D}) = 0$), it is also possible to detail the term of advection $div(\vec{J}_{adv})$:

$$\vec{J}_{adv} = \rho_w C_w \vec{v}_D \cdot T \quad \text{(A1.6a)}$$

$$div(\vec{J}_{adv}) = \rho_w C_w \vec{v}_D \cdot \nabla T \quad \text{(A1.6b)}$$

where $\vec{v}_D$ is the groundwater flow velocity (m/s) and ∇T the thermal gradient (K/m). Regarding the Equations (A1.4), Equation (A1.6b) becomes:

$$div(\vec{J}_{adv}) = -\frac{\rho_w C_w}{\lambda_{eff}} \vec{v}_D \cdot \vec{J}_{cond} \quad \text{(A1.7)}$$

This analysis provides the Peclet number which is a dimensionless number representing the ratio of advection to conduction during heat transfer.

$$P_e = \frac{\rho_w C_w}{\lambda_{eff}} \cdot \|\vec{v}_D\| \cdot L \quad \text{(A1.8)}$$

where L represents the characteristic length of the system (m).

From Equations (A1.3) and (A1.7), it is possible to define the term of conduction.

$$div(\vec{J}_{cond}) = \frac{\rho_w C_w}{\lambda_{eff}} \vec{v}_D \cdot \vec{J}_{cond} - C_{eff} \frac{\partial T}{\partial t} \quad \text{(A1.9)}$$

Appendix 2: test of numerical implementation

The numerical implementation of the DCV approach is checked by comparison with a simple 1D case. The analysis of equation (A1.3) in 1D in steady state conditions provides the following analytical solutions:

$$T(x) = T_1 + \frac{(T_1 - T_0)}{1 - e^{-A \times D}} (e^{-A \times x} - 1) \quad \text{(A2.1)}$$

$$div(\vec{J}_{cond}) = -A^2 \lambda_s \left(\frac{(T_1 - T_0)}{1 - e^{-A.D}} \times e^{-A.x} \right) = -div(\vec{J}_{adv}) \quad \text{(A2.2)}$$

where $T_1$and T_0 are the temperature of the two boundaries (°C), D is the total length (m), x is the position (m) and A is a constant (m^{-1}). A is defined as:

$$A = -\frac{\rho_w C_w}{\lambda_s} \cdot \|\vec{v}_D\| \quad \text{(A2.3)}$$

The numerical model represents a horizontal profile of soil. The parameters chosen for the calculation are listed in the Table A2.1. The temperature is fixed on left and right side to respectively 35°C and 15°C, other boundaries are adiabatic and a groundwater flow from right to left side with a velocity of 5.10^{-7} m/s. Calculations are performed until steady state conditions (Figure A2.1) in order to compare this result to the analytical solution of equations (A2.1) and (A2.2) (Figure A2.2).

Regarding these results, the numerical curves fit satisfactorily with the analytical ones proving the efficient implementation for 1D case. It also shows that with these input parameters there is no temperature variation beyond 4 m. This limit mainly depends on the temperature of the heat source and the groundwater flow velocity which restrains the thermal diffusion.

Moreover, the numerical analysis of the evolution of the divergence with time highlights the zones where the temperature varies the most. Its sign is negative, which means that the temperature is increasing and its value tends to zero after some months proving that steady state is reached (Figure A2.3).

List of figures

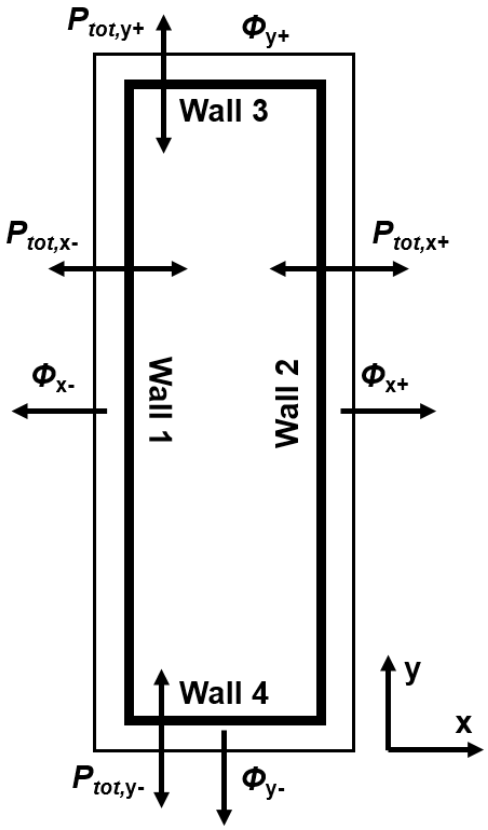

Figure 1: Heat exchanges around a metro station

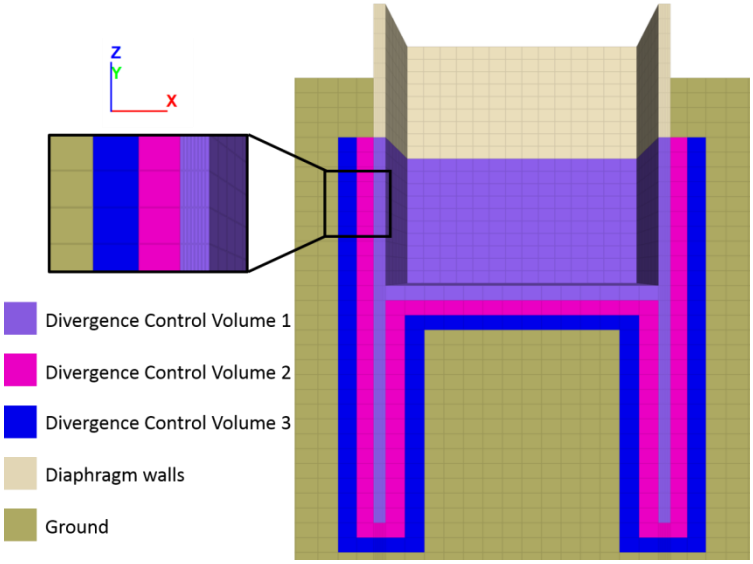

Figure 2: Example of Divergence Control Zone around diaphragm wall

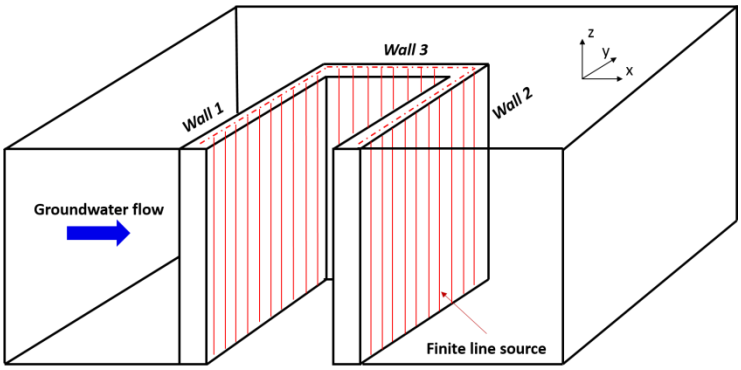

Figure 3: Finite line sources positions in the diaphragm walls

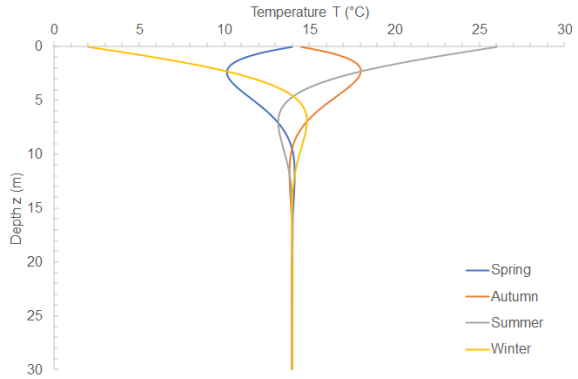

Figure 4: analytical profile of seasonal variation of ground temperature

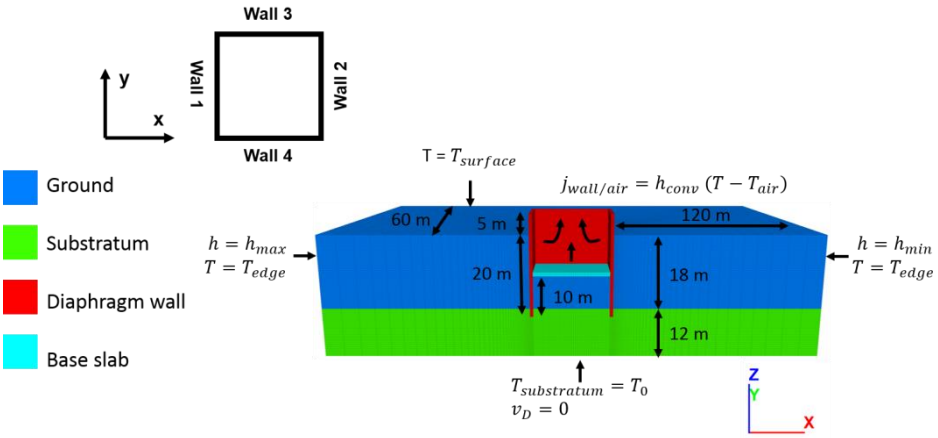

Figure 5: geometry and boundary conditions of the example 1

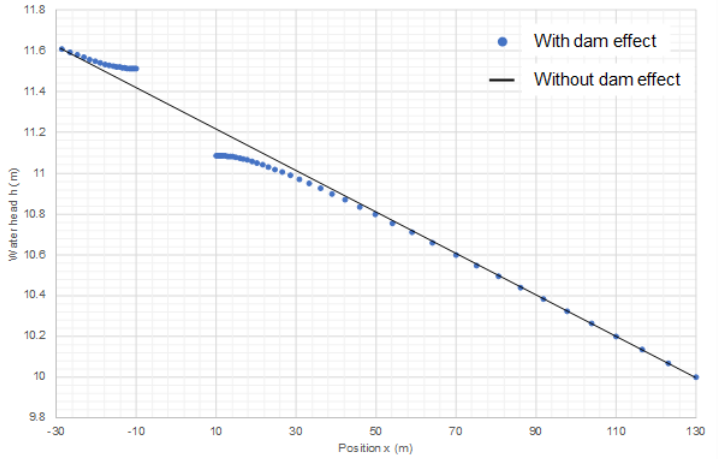

Figure 6: dam effect at a depth of 9 m (i = 1%) – example 1

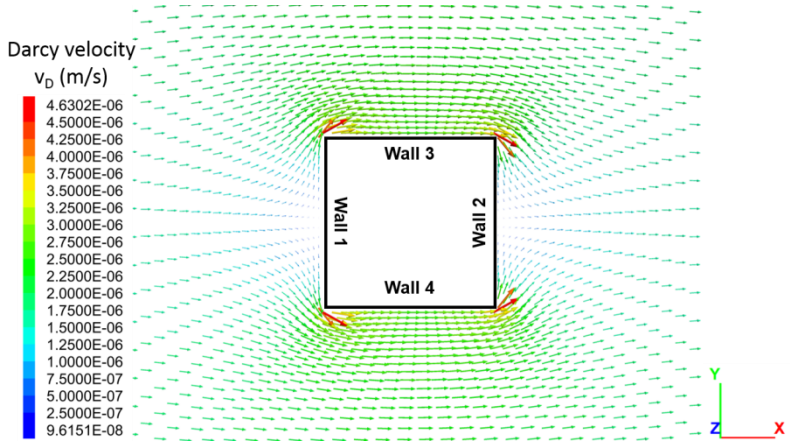

Figure 7: map of groundwater flow velocity – Dam effect – example 1

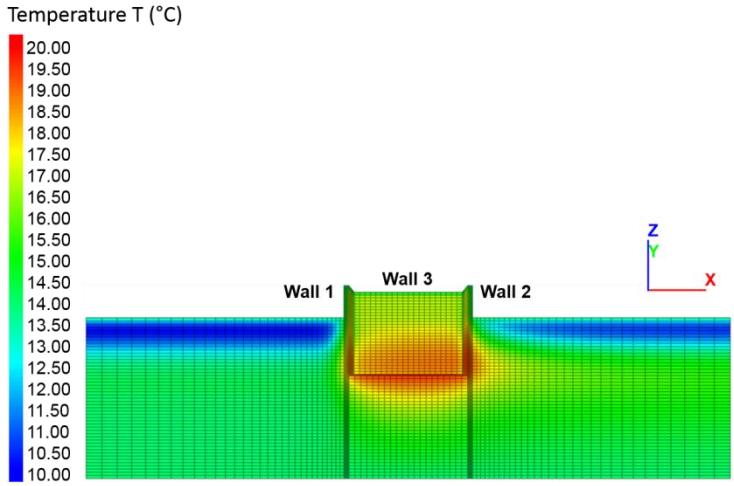

Figure 8: temperature field before geothermal activation – example 1

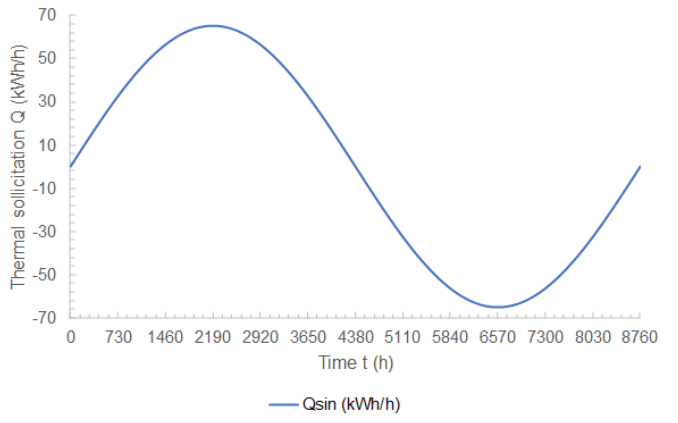

Figure 9: thermal solicitation for the example 1

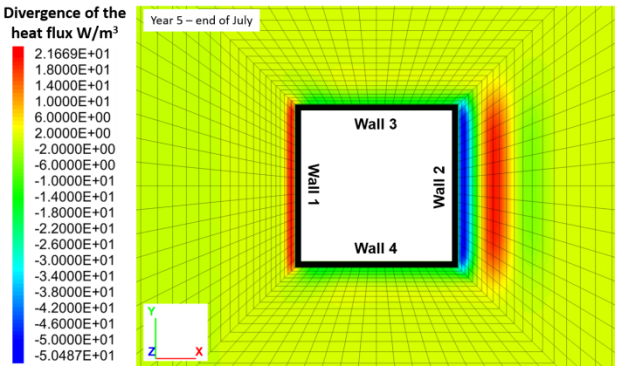

Figure 10: Divergence map at 9 m depth – example 1

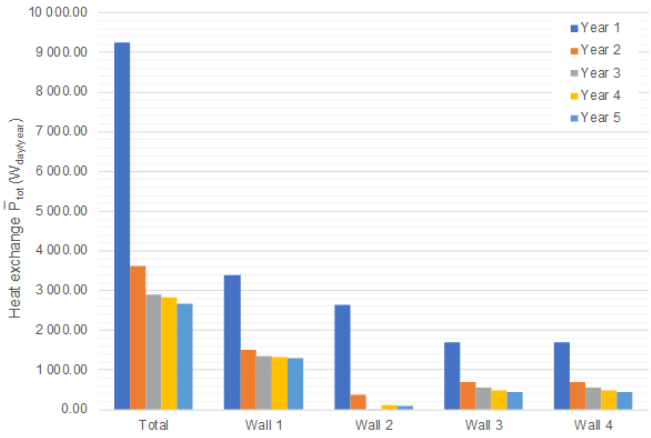

Figure 11: Heat exchange based on the divergence approach – example 1

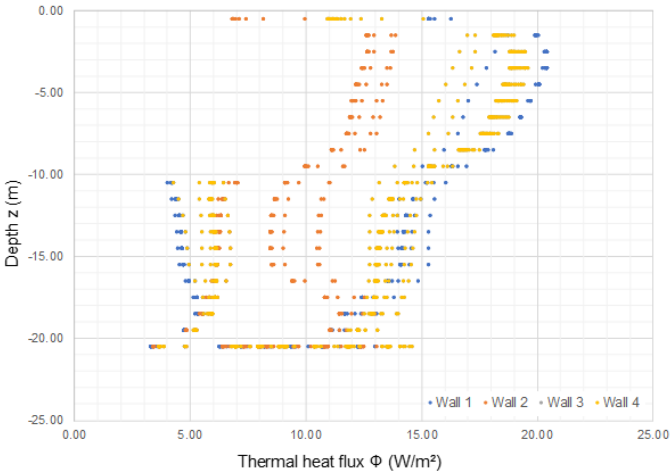

Figure 12: heat flux at the end of July of the year 1 according to the depth – example 1

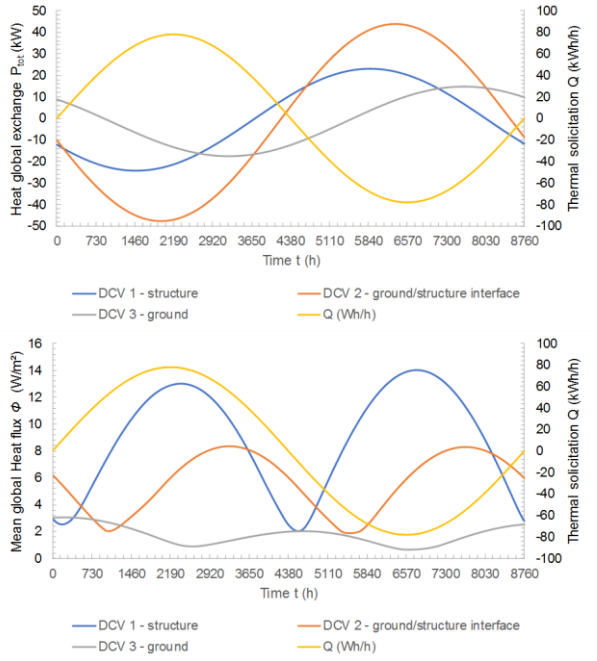

Figure 13: Heat diffusion through the DCV during the third year

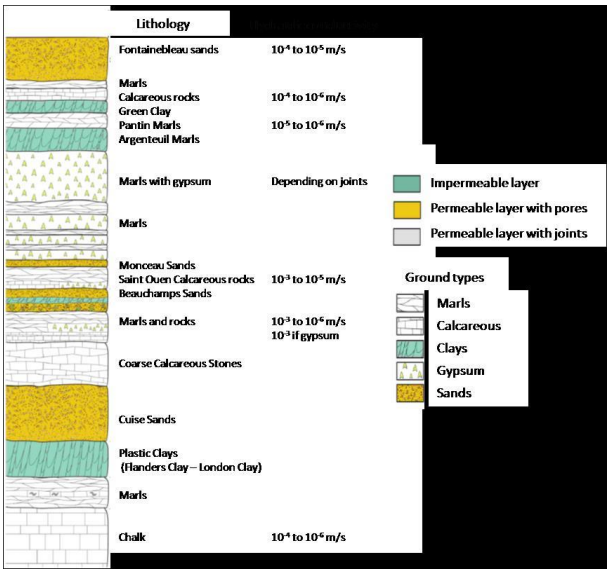

Figure 14: Geology and hydraulic conductivity of Paris

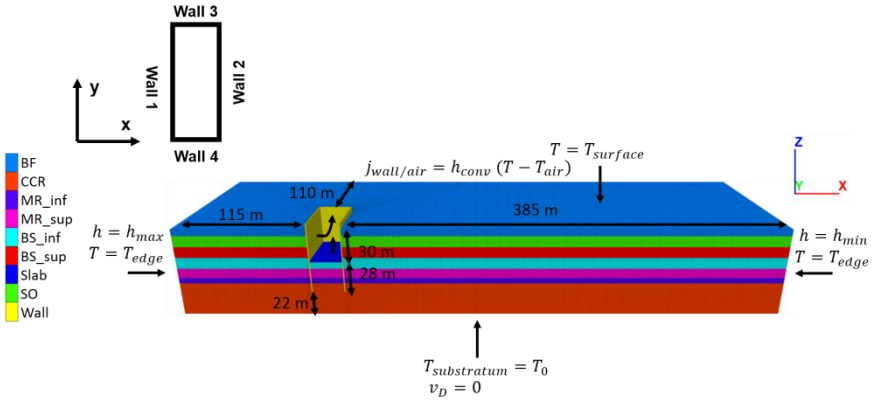

Figure 15: Geometry, geology and boundary conditions for the example 2

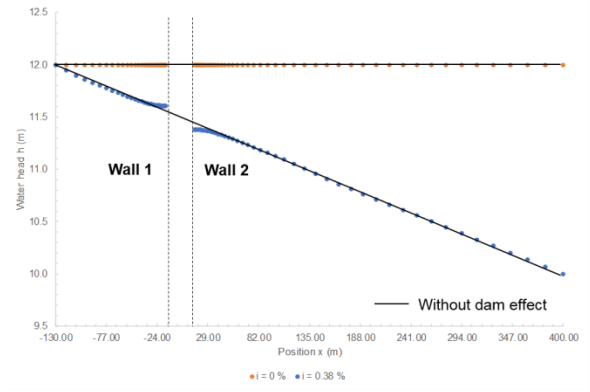

Figure 16: Dam effect at a depth of 15 m (i = 0% and i = 0.38%) – example 2

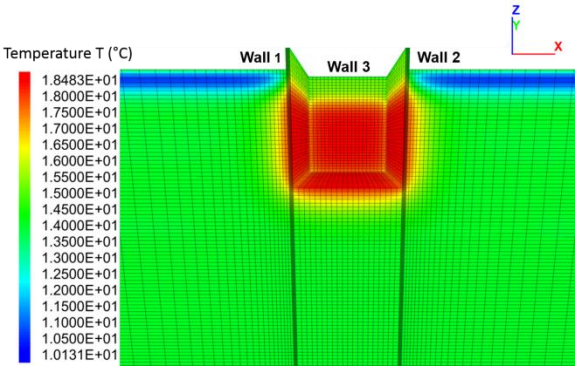

Figure 17: temperature field before geothermal activation – example 2

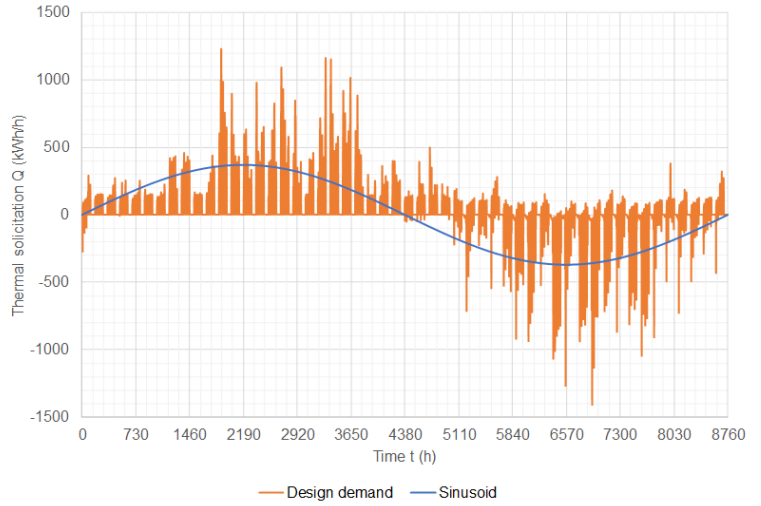

Figure 18 : thermal solicitations for the example 2

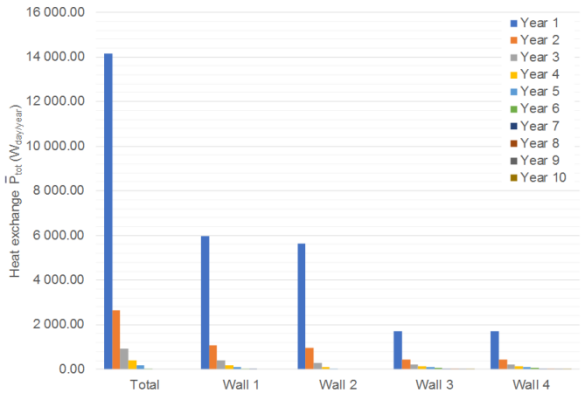

Figure 19: Annual mean of the divergence of the heat flux for each wall – example 2 sinusoidal signal

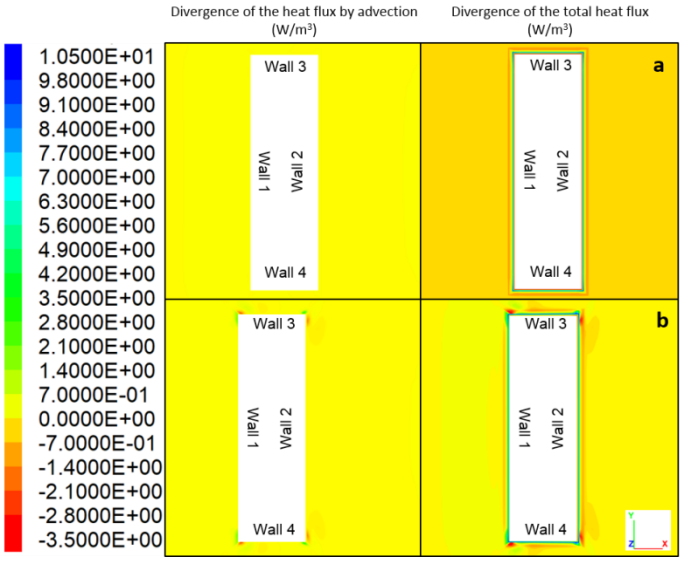

Figure 20 : divergence map of the total heat flux and the heat flux by advection: (a) at 20 m depth, (b) at 40 m depth – example 2

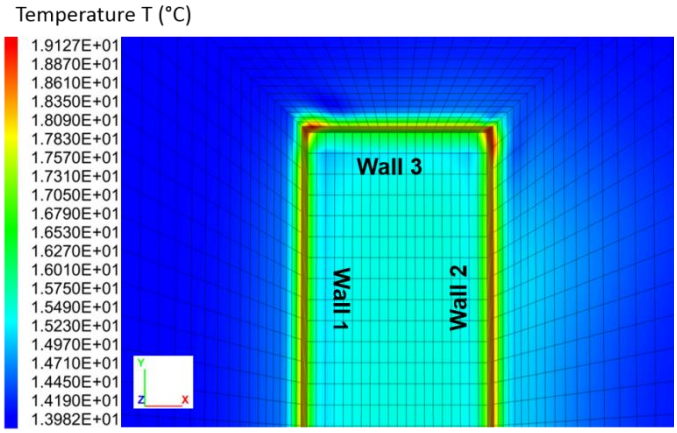

Figure 21: Temperature field at 40 m depth – example 2

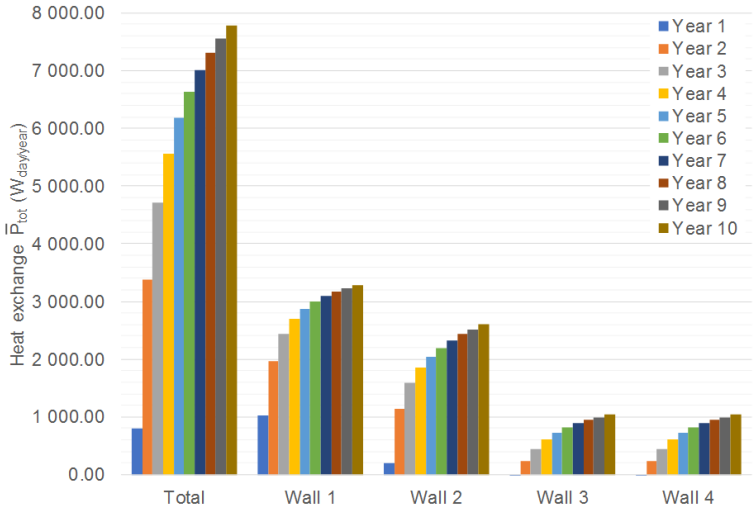

Figure 22: Annual mean of the divergence of the heat flux for each wall – example 2 real signal

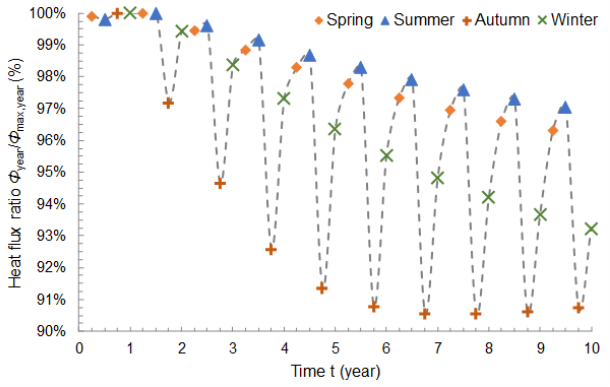

Figure 23: Variation of heat flux ratio over time for the wall 1

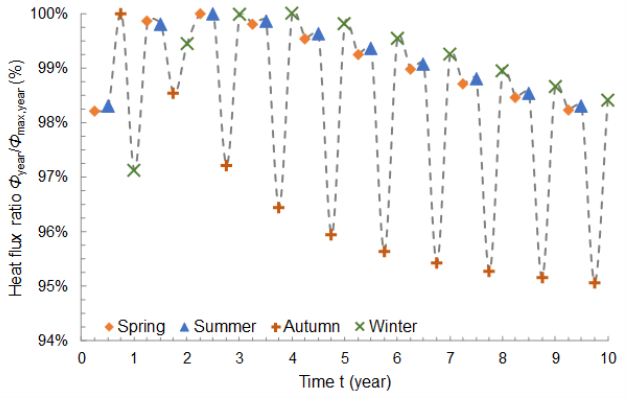

Figure 24: Variation of heat flux ratio over time for the wall 4

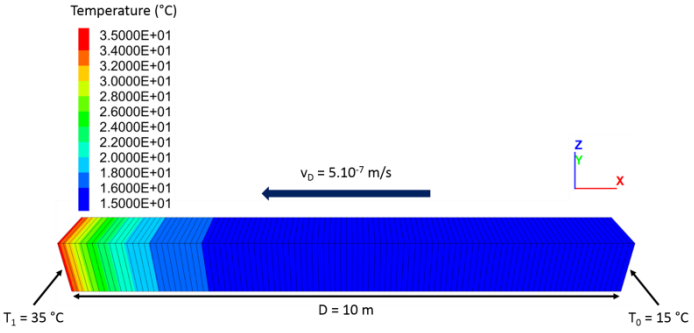

Figure A2.1: Verification of DCV method on a 1D model

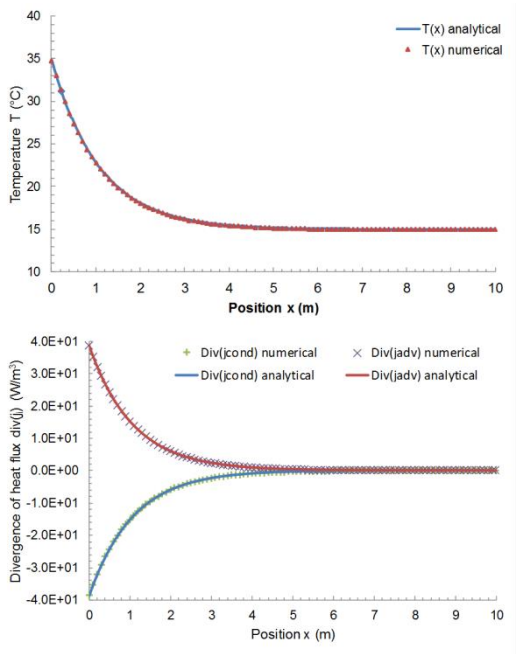

Figure A2.2: DCV approach – comparison between analytical and numerical results in 1D

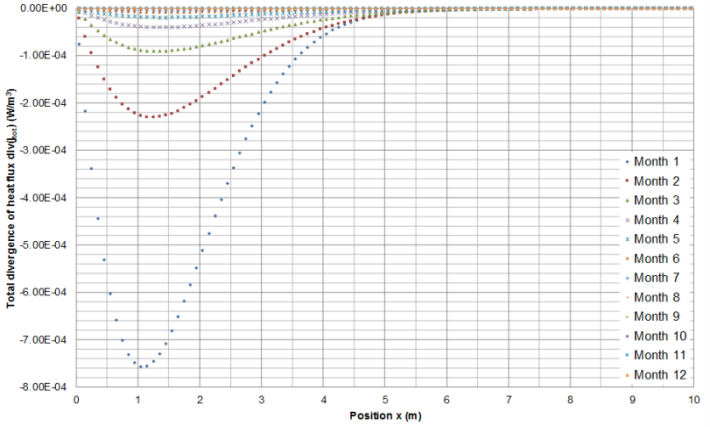

Figure A2.3. Variation of divergence over time in a horizontal profile of soil